Stress-free morphing by means of compatible distortions

Ivan Colorado-Cervantes ⓘ, Valerio Varano ⓘ, and Luciano Teresi ⓘ[*]

Dipartimento di Matematica e Fisica, Università degli Studi Roma Tre, Via della Vasca Navale 84 - 00146 - Rome, Italy

We study the morphing of three-dimensional objects within the framework of nonlinear elasticity with large distortions. A distortion field induces a target metric, and the configuration which is effectively realized by a material body is the one that minimizes the distance, measured through the elastic energy, between the target metric and the actual one. Morphing through distortions might have a paramount feature: the resulting configurations might be stress-free; if this is the case, the distortions field is called compatible. We maintain that the morphing through compatible distortions is a key strategy exploited by many soft biological materials, which can exhibit very large shape-change in response to distortions controlled by stimuli such as chemicals or temperature changes, while keeping their stress state almost null. Thus, the study of compatible distortions, and of the related shape-changes, is quite important. Here, we show a blueprint for stress-free morphing based on the notions of metric tensor and of Riemann curvature which can be used to design large morphing of three-dimensional objects.

I. INTRODUCTION

Since centuries, the main interest of solid mechanics has been the prediction of the strain and the stress state of solids under loadings.

Then, the pioneering works of Refs. [1,2] about the effects of thermal distortions paved the way for an additional research field, the evaluation of the strain and the stress state of unloaded solids under geometrical frustration. The notion of distortions, also known as anelastic strains, proved to be extremely fruitful in modeling crystalline plasticity, based on the idea of the multiplicative composition of the actual strain with the inelastic one [3–6]; the history of this decomposition can be retraced in Ref. [7].

More recently, the theory of nonlinear elasticity with large distortions, also known as anelasticity, from the seminal paper [8] has been applied to study the morphing of elastic bodies, and has been enriched by many new ideas; among them, we cite the introduction of a balance law for the time evolution of distortions and the study of stress-driven remodeling [9,10], the notion of target metric [11,12], and of elastic metric [13], the usage of these modeling tools to the study of biological growth [14–17].

Shape-morphing of two-dimensional (2D) bodies has been extensively studied in the recent decade, both from the theoretical point of view [18–20] and from the point of view of morphing design [21–24]. The notion of distortions has also been widely used to model shape formation of liquid crystal elastomers in the framework of a fully three-dimensional (3D) theory [25–27], or with 2D shell models [28–31].

Design of morphing is now at the core of many applications, and our paper investigates about the possibility of designing stress-free morphing for 3D bodies, following Ref. [32]. The uniqueness of distortion-induced deformations is due to the existence of a special class of distortion fields known as *compatible*, which yield stress-free morphings; on the other hand, deformations caused by loadings will always be stressed.

We support that morphing through compatible distortions is a key strategy exploited by nature, enabling living organisms to perform vital tasks such as changing shape, moving, and adapting to the environment [33–36]. Mimicking the dynamics of these structures by using active materials has been useful in the design of smart systems for engineering applications, i.e., actuation in robotics, foldable electronics, deployable structures, and biomedical applications to name a few [37]; design of shape-morphing has also been addressed for living composites [38,39].

In this work, we explore the possibility of deforming elastic 3D bodies through distortions with the aim to propose a blueprint for the characterization of compatible metric tensors to which there correspond a sought shape transformation, that is, a 3D morphing towards a target shape, realized at zero stress.

Actually, there are plenty of papers about the morphing of shells based on the notion of 2D target metric, and discussing the possible rise of self stresses. Our paper tackles the same problem for 3D bodies and yields explicit representations of many examples of compatible metrics grouped in different families. The anticipated families of shapes that could be created is limitless: our method starts from the explicit representation of some prototypical deformations and then generalizes it basing on the notion of Riemann curvature; moreover, it can be extended to many other more general morphing problems.

Here we discuss ribbons as they have a simple, yet not trivial reference geometry; nevertheless, they yield a large

---

[*]luciano.teresi@uniroma3.it

family of different deformations. Also, ribbons are interesting, not only because of the wide range of different morphings they can generate, but also because there are many "physical" examples or applications as artificial actuators exhibiting motions from flat configurations to curved ribbons and back.

Our approach has limitations; here we list some of them: (a) The formations of sharp corners, or discontinuity in the curvature, cannot be described. (b) Once a compatible metric has been found, its square root might be difficult or impossible to compute explicitly. (c) Our method is granted for simply connected domains; its effectiveness for nonsimply connected domains should be discussed.

The paper is organized as follows: at first, we recapitulate the key notions of nonlinear elasticity with large distortions; we introduce the notions of target and elastic metric, and we present the stress-strain relations in presence of large distortions. Then, we address the compatibility problem for a target metric based on the notion of the Riemann curvature tensor; we propose a way to design a shape morphing and to characterize compatible distortions [16,40]; we give the guidelines to build a compatible distortions starting from a three-dimensional embedding that describes the deformation. Finally, we present a collection of simple compatible distortions which produce stress-free morphing; moreover we validate them numerically using the finite element method (FEM).

II. ELASTICITY WITH DISTORTIONS

In this section we briefly review the theory of nonlinear, 3D elasticity with large distortions [13]. Let $\mathscr{E}$ be the 3D Euclidean ambient space; we denote by $V\mathscr{E}$ its associated vector space, and with $\mathrm{Lin} = V\mathscr{E} \otimes V\mathscr{E} = \mathrm{Sym} \oplus \mathrm{Skw}$ the space of double tensors on $V\mathscr{E}$ (linear maps of $V\mathscr{E}$ into itself). Finally, $\mathrm{Rot} \subset \mathrm{Lin}$ is the space of the orthogonal transformations of $V\mathscr{E}$.

To ease notation, in most of our paper we shall use an Euclidean frame, and thus we do not tell between covariant and contravariant components of vectors and tensors; see Appendix A. Our Euclidean frame is $\{o; \mathbf{e}_1, \mathbf{e}_2, \mathbf{e}_3\}$, with o being the origin and $\mathbf{e}_i$ being three orthonormal vectors of $V\mathscr{E}$. A point of $\mathscr{E}$ is $x = (x_1, x_2, x_3)$, and $x_1\mathbf{e}_1 + x_2\mathbf{e}_2 + x_3\mathbf{e}_3$ is its position vector. A basis of Lin is given by $\mathbf{e}_j \otimes \mathbf{e}_i$, with $i, j = 1, 2, 3$.

A. Kinematics

Given a 3D body $\mathscr{B}$, we define the placement of the body a smooth embedding of $\mathscr{B}$ onto $\mathscr{E}$, described by the map

$$
\begin{aligned}
f : \mathscr{B} &\to \mathscr{E}, \\
x &\mapsto y = f(x) = x + \mathbf{u}(x),
\end{aligned}
\tag{1}
$$

associating any *material point* $x \in \mathscr{B}$ to its position $y = f(x) \in \mathscr{E}$ in space. The vector-valued field $\mathbf{u} = u_i(x)\mathbf{e}_i$ is the displacement field, thus, $y_i = f_i(x) = x_i + u_i(x)\mathbf{e}_i$; finally $f(\mathscr{B})$ describes the actual configuration of $\mathscr{B}$. Given a point x and a placement f, the associated key geometrical functions *gradient $\mathbf{F}$*, *cofactor $\mathbf{F}^*$*, and *Jacobian determinant J* are de-

fined as

$$
\mathbf{F} := \nabla f = \mathbf{I} + \nabla \mathbf{u}, \quad \mathbf{F}^* := J\mathbf{F}^{-\top}, \quad J := \det(\mathbf{F}), \tag{2}
$$

with $\nabla f = \partial f_i / \partial x_j \mathbf{e}_i \otimes \mathbf{e}_j$.

1. Distortions

The important notion of *distortion* has been proposed in the framework of plasticity to describe the natural state of volume elements. Distortions are described by the tensor-valued field

$$
\mathbf{F}_o : \mathscr{B} \to \mathrm{Lin}(T_x\mathscr{B}, T_x\mathscr{B}), \tag{3}
$$

where $T_x\mathscr{B}$ is the tangent space to $\mathscr{B}$ at x, called the *body element* at x. It is worth noting that the deformation gradient $\mathbf{F}$ is a purely kinematical notion; in contrast, the notion of the distortion $\mathbf{F}_o$ has a twofold nature: kinematics and dynamics. In fact, $\mathbf{F}_o$ represents an additional state variable, as it adds nine more degrees of freedom; moreover, it is aimed at describing the *stress-free* state of volume elements; that is, it relies on the notion of stress and some constitutive information on it [9].

Thus, the use of the synonymous terms natural, stress-free, or relaxed, does more than foresee the specification of any free energy: it emphasizes the fact that a distortion has no effect on the value of the free energy of a body element.

The difference between the actual deformation gradient $\mathbf{F}$ and the distortion $\mathbf{F}_o$ is measured through the elastic deformation $\mathbf{F}_e$,

$$
\mathbf{F}_e = \mathbf{F}\mathbf{F}_o^{-1}. \tag{4}
$$

The idea of a multiplicative decomposition $\mathbf{F} = \mathbf{F}_e\mathbf{F}_o$ of $\mathbf{F}$ into the product of an elastic part $\mathbf{F}_e$ and an inelastic (also called plastic) part $\mathbf{F}_o$ is commonly associated with the names of Bilby, Kröner, and Lee [3–5].

2. Strain measures

Given the three tensor fields $\mathbf{F}$, $\mathbf{F}_o$, and $\mathbf{F}_e$, it is possible to define the following metric tensors, having the role of the right Cauchy-Green strain measures:

$$
\begin{aligned}
\mathbf{C} &= \mathbf{F}^\top \mathbf{F}, & \text{actual metric given by } f, \\
\mathbf{C}_o &= \mathbf{F}_o^\top \mathbf{F}_o, & \text{natural metric associated to } \mathbf{F}_o, \\
\mathbf{C}_e &= \mathbf{F}_e^\top \mathbf{F}_e, & \text{elastic metric evaluated with } \mathbf{F}_e.
\end{aligned}
\tag{5}
$$

In general, $\mathbf{C}_o$ is not Euclidean; that is, flat Riemannian, but Riemannian in the general sense; this attribute comes from the fact that $\mathbf{F}_o$ is not necessarily compatible; that is, it might not exist an embedding f such that $\nabla f = \mathbf{F}_o$.

Incompatible distortions would cause body elements to overlap or tear; to avoid that, body elements must be elastically deformed to compensate for the lack of compatibility. The metric tensor measuring this elastic deformation is the elastic metric $\mathbf{C}_e$, which can be represented as a multiplicative difference between $\mathbf{C}$ and $\mathbf{F}_o$,

$$
\mathbf{C}_e = \mathbf{F}_e^\top \mathbf{F}_e = \mathbf{F}_o^{-\top}\mathbf{C}\mathbf{F}_o^{-1}. \tag{6}
$$

Based on $\mathbf{C}_e$, it is possible to define other classical strain measures used in solid mechanics, such as the Green Saint-Venant strain $\mathbf{E}_e$, defined by

$$
\mathbf{E}_e = \tfrac{1}{2}(\mathbf{C}_e - \mathbf{I}). \tag{7}
$$

$$\mathbf{T} = J^{-1}\,\mathbf{S}\,\mathbf{F}^T$$

$$\mathbf{F}$$

$$\mathbf{F}_e = \mathbf{F}\,\mathbf{F}_o^{-1}$$

$$\mathbf{S} = \mathbf{T}\,\mathbf{F}^* = \mathbf{S}_o\,\mathbf{F}_o^*$$

$$\psi = J_o\,\psi_o\,, \qquad \mathbf{S}_e = \mathbf{S}_{oe}\,\mathbf{F}_o^*$$

$$\mathbf{F}_o \qquad\qquad \psi_o\,, \qquad \mathbf{S}_{oe} = \frac{\partial \psi_o}{\partial \mathbf{F}_e}$$
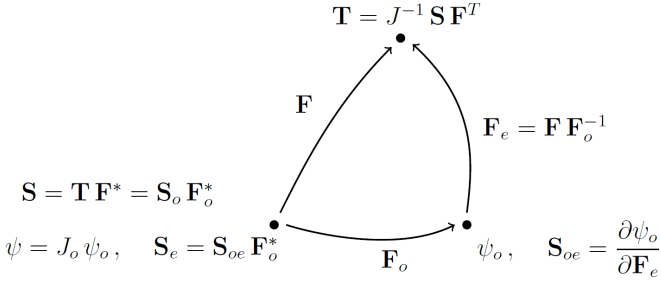
FIG. 1. Stress measures and energy densities are placed in a triangular diagram; pull back and push forward operations are highlighted for each transformation.

Let us note that $\mathbf{E}_e$ is not a metric tensor, not being positive definite, and can be rewritten in terms of the differences $\mathbf{C} - \mathbf{C}_o$ or $\mathbf{E} - \mathbf{E}_o$:

$$\mathbf{E}_e = \mathbf{F}_o^{-\top}\tfrac{1}{2}(\mathbf{C} - \mathbf{C}_o)\mathbf{F}_o^{-1} = \mathbf{F}_o^{-\top}(\mathbf{E} - \mathbf{E}_o)\mathbf{F}_o^{-1}, \qquad (8)$$

with $\mathbf{E} = \tfrac{1}{2}(\mathbf{C} - \mathbf{I})$ and $\mathbf{E}_o = \tfrac{1}{2}(\mathbf{C}_o - \mathbf{I})$. It is this representation that prompts the alias *target metric* for $\mathbf{C}_o$: the strain $\mathbf{E}_e$ measures the deviation of the actual metric $\mathbf{C}$ from the target one $\mathbf{C}_o$.

B. Elastic energy

We consider a hyperelastic response for $\mathscr{B}$, described by a free energy density ψ_o per unit relaxed volume $dV_o = J_o dV$, with dV being the reference volume element on $\mathscr{B}$, and $J_o = \det \mathbf{F}_o$ being the determinant of the linear transformation $\mathbf{F}_o$. Let us note that, by using an orthonormal Euclidean basis, as done in most of our paper, J_o coincides with the determinant of its matrix representation: $J_o = \det(F_{oij})$.

The free energy is assumed to depend on the elastic deformation $\mathbf{F}_e$, that is $\psi_o = \psi_o(\mathbf{F}_e)$. It follows that the strain energy density ψ, per unit reference volume dV, is given by

$$\psi = J_o\psi_o(\mathbf{F}_e). \qquad (9)$$

Standard procedures of continuum mechanics yields the following stress measures, see also Fig. 1:

$$
\begin{aligned}
\mathbf{S}_{oe} &= \frac{\partial \psi_o}{\partial \mathbf{F}_e}, & \text{energetic stress,} \\[4pt]
\mathbf{S}_e &= \mathbf{S}_{oe}\mathbf{F}_o^*, & \text{reference stress (Piola-kirchhoff),} \\[4pt]
\mathbf{T}_e &= \mathbf{S}_e(\mathbf{F}^*)^{-1}, & \text{actual stress (Cauchy).}
\end{aligned}
$$
$$(10)$$

Here, the subscript "e" is meant to highlight the reference to the energetic component of the stress. Additional internal constraints, as incompressibility, would add additional stress terms. Let us note that, by using a different representation of the free energy density $\phi_o = \phi_o(\mathbf{C}_e) = \psi_o(\mathbf{F}_e)$, we have

$$\mathbf{S}_{oe} = 2\mathbf{F}_e\frac{\partial \phi_o}{\partial \mathbf{C}_e} = \mathbf{F}_e\frac{\partial \phi_o}{\partial \mathbf{E}_e}. \qquad (11)$$

The derivative of the energy with respect to $\mathbf{E}_e$ is commonly called second Piola-Kirchhoff stress,

$$\frac{\partial \phi_o}{\partial \mathbf{E}_e} = \mathbf{F}_e^{-1}\mathbf{S}_{oe}. \qquad (12)$$

Finally, the actual stress $\mathbf{T}_e$ can be represented as

$$\mathbf{T}_e = \frac{1}{J}\mathbf{S}_e\mathbf{F}^\top = \frac{1}{J}\mathbf{F}_e\frac{\partial \phi_o}{\partial \mathbf{E}_e}\mathbf{F}_o^*\mathbf{F}^\top = \frac{1}{J_e}\mathbf{F}_e\frac{\partial \phi_o}{\partial \mathbf{E}_e}\mathbf{F}_e^\top. \qquad (13)$$

C. The typical elastic problem

A typical problem of nonlinear elasticity with distortions can be formulated as follows: given an elastic body $\mathscr{B}$, with loadings, constraints, and distortions, find its placement $f : \mathscr{B} \to \mathscr{E}$. The solution f^* to this problem is obtained as a minimization of the elastic energy, where the distortion field $\mathbf{F}_o$ is an input of the problem

$$f^*(.,\mathbf{F}_o) = \min_f \int_{\mathscr{B}} \psi(\mathbf{C}_e)dV. \qquad (14)$$

Due to the presence of the distortions, the strain $\mathbf{C}_e$ can be different from the identity even in the absence of loadings and constraints. Our goal is to design a distortion field $\mathbf{F}_o$ such that f^* is a sought shape, and $f^*(\mathscr{B}, \mathbf{F}_o)$ is a stress-free configuration.

III. COMPATIBILITY

The existence of stress-free configurations generated by the prescription of a compatible distortion field is a subject of tremendous importance within the framework of shape-morphing. These configurations are particular elastic solutions which minimize the elastic energy at zero stress.

A. Riemann curvature tensor

Given a metric tensor $\mathbf{G}$, its associated Riemann curvature $\mathbf{R}(\mathbf{G})$ is made of linear combinations of second derivatives of the components of $\mathbf{G}$; the usual representation of $\mathbf{R}(\mathbf{G})$ is done in terms of the Christoffel symbols.

For all $i, j, k, q \in \{1, 2, 3\}$, let the functions $\boldsymbol{\Gamma}_{ijq}$ and $\boldsymbol{\Gamma}_{ij}^p$ be the Christoffel symbols of the first and second kind, respectively, defined by

$$\boldsymbol{\Gamma}_{ijq} = \tfrac{1}{2}(\partial_j\mathbf{G}_{ij} + \partial_i\mathbf{G}_{jq} + \partial_q\mathbf{G}_{ij}), \qquad (15)$$

and

$$\boldsymbol{\Gamma}_{ij}^p = \mathbf{G}^{pq}\boldsymbol{\Gamma}_{ijq}, \qquad (16)$$

where $\mathbf{G}^{pq} = \mathbf{G}_{pq}^{-1}$. Then, the Riemann curvature tensor associated with $\mathbf{C}$ is given by

$$\mathbf{R}_{qijk} = \partial_j\boldsymbol{\Gamma}_{ikq} - \partial_k\boldsymbol{\Gamma}_{ijq} + \boldsymbol{\Gamma}_{ij}^p\boldsymbol{\Gamma}_{kqp} - \boldsymbol{\Gamma}_{ik}^p\boldsymbol{\Gamma}_{jqp}. \qquad (17)$$

In a 3D space, the Riemann tensor has 81 components, but most of them are null or redundant; actually, in 3D, $\mathbf{R}$ can be represented at glance by a 3×3 skew-symmetric matrix, whose entries are 3×3 skew-symmetric matrices, see (18). The skew symmetry implies that only six strict components remain. As this representation shows, the three matrices on the diagonal are null; moreover, all the matrices out of diagonal are skew-symmetric, and have their diagonals null:

$$\mathbf{R} = \begin{bmatrix} \begin{bmatrix} 0 & 0 & 0 \\ 0 & 0 & 0 \\ 0 & 0 & 0 \end{bmatrix} & \begin{bmatrix} 0 & -\mathbf{R}_{1212} & -\mathbf{R}_{1213} \\ & 0 & -\mathbf{R}_{1223} \\ \text{skw} & & 0 \end{bmatrix} & \begin{bmatrix} 0 & -\mathbf{R}_{1312} & -\mathbf{R}_{1313} \\ & 0 & -\mathbf{R}_{1323} \\ \text{skw} & & 0 \end{bmatrix} \\ \begin{bmatrix} 0 & \mathbf{R}_{1212} & \mathbf{R}_{1213} \\ & 0 & \mathbf{R}_{1223} \\ \text{skw} & & 0 \end{bmatrix} & \begin{bmatrix} 0 & 0 & 0 \\ 0 & 0 & 0 \\ 0 & 0 & 0 \end{bmatrix} & \begin{bmatrix} 0 & -\mathbf{R}_{2312} & -\mathbf{R}_{1323} \\ & 0 & -\mathbf{R}_{2323} \\ \text{skw} & & 0 \end{bmatrix} \\ \begin{bmatrix} 0 & \mathbf{R}_{1312} & \mathbf{R}_{1313} \\ & 0 & \mathbf{R}_{1323} \\ \text{skw} & & 0 \end{bmatrix} & \begin{bmatrix} 0 & \mathbf{R}_{2312} & \mathbf{R}_{2313} \\ & 0 & \mathbf{R}_{2323} \\ \text{skw} & & 0 \end{bmatrix} & \begin{bmatrix} 0 & 0 & 0 \\ 0 & 0 & 0 \\ 0 & 0 & 0 \end{bmatrix} \end{bmatrix}. \tag{18}$$

Moreover, due to major symmetry, $\mathbf{R}_{1312} = \mathbf{R}_{1213}$, $\mathbf{R}_{2312} = \mathbf{R}_{1223}$, and $\mathbf{R}_{1323} = \mathbf{R}_{2313}$. Consequently, the equation $\mathbf{R}(\mathbf{C}) = 0$ consists of six partial differential equations involving the six strict components of $\mathbf{C}$; this system of six PDEs might be used as a tool to characterize compatible fields $\mathbf{F}_o$.

We conclude this section by noting that, due to the two minor skew-symmetry and the major symmetry, in 3D the forth-order tensor $\mathbf{R}$ can be represented by two different symmetric tensors of order two, the incompatibility tensor, and the Ricci tensor. The first one is defined by means of the axial vector operator [41]; the second one is defined through a double contraction of the indices of the Riemann tensor [42]. Here, in order to maintain the meaning, we prefer the notation with the four indices.

B. Compatible distortions

Given a smooth, positive definite, symmetric tensor field $\mathbf{G}$ on a simple-connected domain $\mathscr{B}$, the necessary and sufficient condition for $\mathbf{G}$ to be the *metric tensor* of a realizable configuration is that its associated Riemann curvature tensor $\mathbf{R} = \mathbf{R}(\mathbf{G})$ be null [40]; we have

$$\mathbf{R}(\mathbf{G}) = 0 \Leftrightarrow \exists f : \mathscr{B} \to \mathscr{E} \text{ s.t. } \nabla f^\top \nabla f = \mathbf{G}. \tag{19}$$

Moreover, the embedding f is *unique* up to a global isometry, and $\mathbf{G}$ is called Euclidean metric tensor. The same test can be done on the natural metric $\mathbf{C}_o$ to assess the compatibility of $\mathbf{F}_o$, that is

$$\mathbf{R}(\mathbf{C}_o) = 0 \Leftrightarrow \exists f : \mathscr{B} \to \mathscr{E} \text{ s.t. } \nabla f = \mathbf{F}_o, \tag{20}$$

and the natural metric $\mathbf{C}_o$ is Euclidean; the configuration $f(\mathscr{B})$ is realizable and unique up to isometries, provided that the map f satisfies possible boundary conditions.

A discussion about the generalization of (20) for arbitrary nonsimply connected bodies can be found in Ref. [43]. Let us now consider the polar decomposition of ∇f and $\mathbf{F}_o$ into symmetric and orthogonal components

$$\nabla f = \mathbf{Q}\mathbf{U} \text{ and } \mathbf{F}_o = \mathbf{Q}_o\mathbf{U}_o. \tag{21}$$

The vanishing of the Riemann curvature associated with $\mathbf{C}_o$ implies the existence of a unique placement f in which only the symmetric components of ∇f and $\mathbf{F}_o$ are equal

$$\mathbf{R}(\mathbf{C}_o) = 0 \Leftrightarrow \left(\nabla f^\top \nabla f\right)^{1/2} = \mathbf{U} = \mathbf{U}_o = \left(\mathbf{F}_o^\top \mathbf{F}_o\right)^{1/2}. \tag{22}$$

Consequently, the compatibility of $\mathbf{F}_o$ has the following implications [13]:

(1) The elastic deformation $\mathbf{F}_e$ reduces to a rotation

$$\mathbf{F}_e = \nabla f \mathbf{F}_o^{-1} = \mathbf{Q}\mathbf{U}\mathbf{U}_o^{-1}\mathbf{Q}_o^\top = \mathbf{Q}\mathbf{Q}_o^\top; \tag{23}$$

thus, the elastic metric is the identity, and the elastic stress is identically null:

$$\mathbf{C}_e = \mathbf{F}_e^\top \mathbf{F}_e = \mathbf{I} \Rightarrow \frac{\partial \psi_o(\mathbf{I})}{\partial \mathbf{F}_e} = 0. \tag{24}$$

(2) The set of all compatible distortions sharing the same metric $\mathbf{C}_o$ constitutes an equivalent class [9,41]. Given a compatible distortion $\mathbf{F}_o$, the product $\mathbf{Q}\mathbf{F}_o$, for any $\mathbf{Q} \in \text{Rot}$, is also compatible, as both yield the same natural metric.

IV. MORPHING DESIGN

In this section we illustrate our proposal for morphing design which relies on the construction of compatible distortions aimed at generating a stress-free target shape. Our approach is based on the following algorithm: at first, we construct a 3D embedding by extruding a curve f_c to a surface f_s, and then to a volume f; this procedure can generate a great collection of different parametric configurations.

Then, we compute the metric $\mathbf{C}$ of this embedding and extract its square root $\mathbf{U} = \sqrt{\mathbf{C}}$, meant to represent a prototypical distortion $\mathbf{U}_o$, compatible by construction. Finally, we modify the prototypical distortion to $\tilde{\mathbf{U}}_o$ and solve the Riemann curvature equation $\mathbf{R}(\tilde{\mathbf{U}}_o^2) = 0$ to characterize the modifications which maintain the compatibility. At a glance, we have

$$f \to \nabla f \to \mathbf{C} = \nabla f^\top \nabla f \to \mathbf{U} = \sqrt{\mathbf{C}} = \mathbf{U}_o, \text{ prototype;}$$

$$\mathbf{U}_o \to \tilde{\mathbf{U}}_o, \text{ modification of prototype;}$$

$$\tilde{\mathbf{U}}_o \to \mathbf{R}(\tilde{\mathbf{U}}_o^2) = 0 \to \text{compatible} \tilde{\mathbf{U}}_o \to \text{integration} \tilde{f}. \tag{25}$$

In the absence of loads and constraints, both $f(\mathscr{B})$ and $\tilde{f}(\mathscr{B})$ are stress-free configurations.

A. Extruding a three-dimensional solid from a curve

Let $y = f_c(x_1)$ be a curve parametrized by a one-dimensional (1D) interval; the Frenet-Serret frame of the curve is given by the triad of unit vectors $\{\mathbf{t}, \mathbf{n}, \mathbf{b}\}$, attached at $y = f_c(x_1)$. The tangent $\mathbf{t}$, the normal $\mathbf{n}$, and the binormal $\mathbf{b}$ are defined by

$$\mathbf{t} = \frac{f_c'}{\lambda}, \quad \mathbf{n} = \frac{\mathbf{t}'}{|\mathbf{t}'|}, \quad \mathbf{b} = \mathbf{t} \times \mathbf{n}, \tag{26}$$

where the prime denotes the derivative d/dx_1 and $\lambda = |f'_c|$ is the axial *stretch*. From (26), it is possible to define the *curvature* κ and the *torsion* τ as follows:

$$\kappa = \frac{|\mathbf{t}'|}{\lambda} = \frac{|f'_c \times f''_c|}{|f'_c|^3}, \quad \tau = \frac{|\mathbf{b}'|}{\lambda} = \frac{f'_c \times f''_c \cdot f'''_c}{|f'_c \times f''_c|^2}. \quad (27)$$

It is worth noting that the relevant geometric information about the curve f_c is summarized by the three scalars $\{\lambda, \kappa, \tau\}$. We now extrude the 1D curve f_c along the binormal direction to get a 2D ruled surface f_s:

$$y = f_s(x_1, x_2) = f_c(x_1) + x_2 \mathbf{b}(x_1). \quad (28)$$

Then, we extrude the 2D surface f_s along its normal direction $\mathbf{n}_s$ to obtain a 3D solid f:

$$y = f(x_1, x_2, x_3) = f_s(x_1, x_2) + x_3 \mathbf{n}_s(x_1, x_2), \quad (29)$$

where $\mathbf{n}_s$ is the normal to the surface f_s and is given by

$$\mathbf{n}_s = \frac{f_{s,1} \times f_{s,2}}{|f_{s,1} \times f_{s,2}|}, \quad (30)$$

with $f_{s,i} = \partial f_s / \partial x_i$. The gradient ∇f of the embedding (29) takes the following form:

$$\mathbf{F} = \nabla f = \nabla f_s + x_3 \nabla \mathbf{n}_s + \mathbf{n}_s \otimes \mathbf{e}_3, \quad (31)$$

to which we can give a matrix-like representation

$$[\mathbf{F}] = [\ \nabla f_s \ | \ \mathbf{n}_s \ ] + x_3 [\ \nabla \mathbf{n}_s \ | \ 0 \ ]. \quad (32)$$

The metric tensor $\mathbf{C} = \mathbf{F}^\top \mathbf{F}$ associated with (31) has the following matrix-like representation

$$[\mathbf{C}] = \left[\begin{array}{c|c} \mathbf{A} & \cdot \\ \hline \cdot & 1 \end{array}\right] + x_3 \left[\begin{array}{c|c} 2\mathbf{B} & \cdot \\ \hline \cdot & \cdot \end{array}\right] + x_3^2 \left[\begin{array}{c|c} \nabla \mathbf{n}_s^\top \nabla \mathbf{n}_s & \cdot \\ \hline \cdot & \cdot \end{array}\right], \quad (33)$$

from which it is possible to identify the three *fundamental forms* (FFs) of the surface f_s; these FFs can be represented in terms of the geometric parameters $\{\lambda, \kappa, \tau\}$. The first FF is given by

$$[\mathbf{A}] = \nabla f_s^\top \nabla f_s = \begin{bmatrix} \lambda^2 + (x_2\tau)^2 & 0 \\ 0 & 1 \end{bmatrix}. \quad (34)$$

The second FF is given by

$$[\mathbf{B}] = \frac{1}{2}\left(\nabla f_s^\top \nabla \mathbf{n}_s + \nabla \mathbf{n}_s^\top \nabla f_s\right) = \begin{bmatrix} -\kappa\lambda & \dfrac{\tau}{2} \\ \dfrac{\tau}{2} & 0 \end{bmatrix}. \quad (35)$$

Finally, the third FF is given by

$$[\nabla \mathbf{n}_s^\top \nabla \mathbf{n}_s] = \begin{bmatrix} \kappa^2 + \tau^2 & 0 \\ 0 & 0 \end{bmatrix}. \quad (36)$$

B. Representation of general helicoidal solid

We construct the embedding of a 3D parallelepiped onto a helicoidal solid, wound around a cylinder. This embedding, with the due parametrization, can generate a large family of different morphings. The embedding is made by composing two maps:
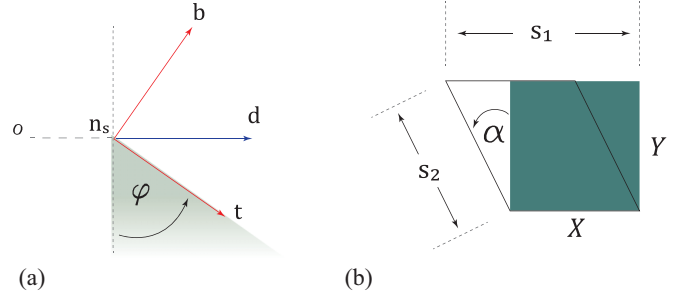
$$x \mapsto s = s(x) \mapsto y = f(s). \quad (37)$$

(a)   (b)

FIG. 2. (left) Helix angle φ between the helix tangent $\mathbf{t}$ and the axis of the cylinder; see also panel (a) of Fig. 3. (right) Effect of the shear $s = s(x)$ described by (38), shown in the plane (x_1, x_2); we set $\lambda_i = 1$.

The first map $s = s(x)$ is a change of coordinates defined by

$$\begin{array}{rcl} s_1 & = & \lambda_1 x_1 + \lambda_2 x_2 \tan\alpha, \\ s_2 & = & x_2 \sec\alpha, \\ s_3 & = & \lambda_3 x_3. \end{array} \quad (38)$$

The parameters λ_i are stretches along x_i; it is important to note that the first two equations represent a shear of the parameters domain of angle α in the plane (x_1, x_2), see Fig. 2, right; this shear identifies the material fiber that will remain straight in the ruled surface of the embedding.

The second map $y = f(s)$ is an embedding defined using an algorithm similar to that described in Sec. IV A: start with a curve f_c, then extrude to a surface f_s, and eventually to a volume f, see Fig. 3. The curve f_c is a helix wound around a cylinder of radius R and axis $\mathbf{e}_2$, and with helix angle φ, given by

$$f_c(s_1) = R\sin\phi\,\mathbf{e}_1 + s_1\sin\varphi\,\mathbf{e}_2 + R(\cos\phi - 1)\mathbf{e}_3, \quad (39)$$

with $\phi = s_1\cos(\varphi)/R$. Both the radius R and the helix angle φ can be represented in terms of the curvature κ and the torsion τ of f_c as follows:

$$R = \frac{\kappa}{\kappa^2 + \tau^2}, \quad \varphi = \arctan(\kappa, \tau), \quad (40)$$

where $\arctan(\kappa, \tau)$ gives the arc tangent of κ/τ, taking into account which quadrant the point (κ, τ) is in. To have more general morphings, the helix f_c is extruded to a surface along the direction

$$\mathbf{d}(s_1) = \cos\theta[\cos\psi\,\mathbf{b}(s_1) + \sin\psi\,\mathbf{t}(s_1)] + \sin\theta\,\mathbf{n}(s_1), \quad (41)$$

represented in term of the Frenet frame $\{\mathbf{t}, \mathbf{n}, \mathbf{b}\}$; here ψ is the angle of a rotation with axis $\mathbf{n}$, and θ represents the Love's torsion [44]. The helicoidal surface f_s is thus given by

$$f_s(s_1, s_2) = f_c(s_1) + s_2 \mathbf{d}(s_1). \quad (42)$$

It is worth noting that in general, due to the fact that the binormal $\mathbf{b}$ does not belong to the tangent plane at the cylinder, the helicoidal surface f_s does not lie on it, i.e., it is not developable. A developable surface is characterized by the request of having vanishing Gaussian curvature; that is, assuming $\det\mathbf{A} \neq 0$, by

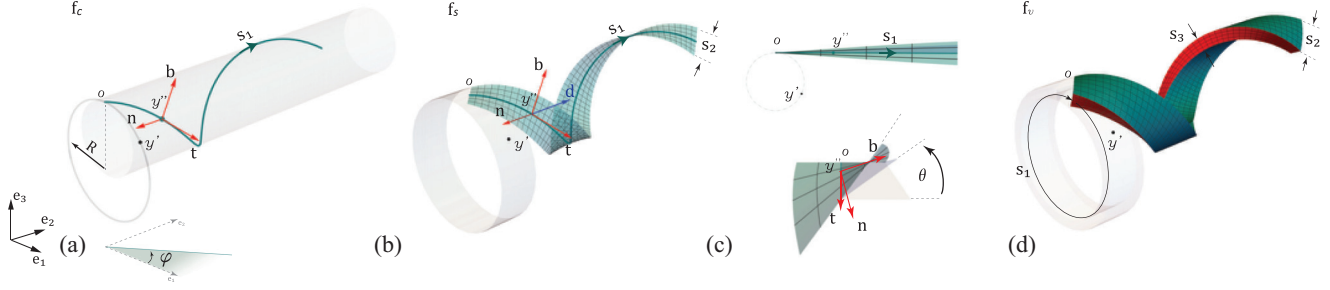$$\det\mathbf{B} = 0 \Leftrightarrow \psi = \varphi. \quad (43)$$

FIG. 3. From left to right: Helix $f_c(s_1)$ around a cylinder; helicoidal Surface $f_s(s_1, s_2)$; helicoidal solid $f(s_1, s_2, s_3)$.

Moreover, f_s has null shear when $\mathbf{A}_{12} = 0$ that is, when $\alpha = -\psi$. Finally, the solid f is given by

$$f(x_1, x_2, x_3) = f_c(s_1) + s_2\mathbf{d}(s_1) + s_3\mathbf{n}_s(s_1, s_2), \quad (44)$$

with $\mathbf{n}_s(s_1, s_2)$ derived from (42) using (30), and $s_i = s_i(x_1, x_2, x_3)$ given by (38). We note that the Frenet frame and the surface normal $\mathbf{n}_s$ are computed by derivatives of f_c and f_s with respect to the parameters s_1, s_2, while the gradient $\mathbf{F} = \nabla f$ has to be computed through derivatives with respect to the coordinates x_i.

Two more parameters are added to f_s by considering $\theta = \theta_o + s_1\theta_1$ in (41); θ_o yields a uniform rotation of the surface around the curve f_c, while θ_1 yields twist along the curve. To highlight all the parameters involved in (44), we rewrite it as follows

$$y = f(x; R, \varphi, \lambda_i, \alpha, \psi, \theta_o, \theta_1). \quad (45)$$

The above 3D parametric embedding is suitable to represents both 3D ribbon-like solids [45–47], sheet-like solids, and beam-like solids [48,49].

V. WORKED EXAMPLES

In the following we shall give some worked examples of the algorithm proposed in Sec. IV; we always assume as reference configuration for $\mathscr{B}$ a parallelepiped having length L, width W and height H:

$$\mathscr{B} = [0, L] \times [-W/2, W/2] \times [-H/2, H/2]. \quad (46)$$

Our twofold approach is based on: (1) the use of the parametrized embedding (44) to generate some interesting shape morphings, and to compute the corresponding distortions $\mathbf{U}_o$; (2) the study of a modification $\tilde{\mathbf{U}}_o$ of a prototypical distortion $\mathbf{U}_o$, in order to make it compatible by solving the equation $\mathbf{R}(\tilde{\mathbf{U}}_o^2) = 0$. We shall use the notation

$$f(\mathscr{B}; \mathbf{U}_o) \quad \text{or} \quad \tilde{f}(\mathscr{B}; \tilde{\mathbf{U}}_o) \quad (47)$$

to highlight the fact that the configurations of $\mathscr{B}$ are parametrized by a distortion field. As byproduct, we solve all our morphings problem using a finite elements analysis to check numerically the existence of the zero-stress states; we note that such nonlinear elastic problems are solved quite easily by the finite elements method.

A. Bending

We start with the simplest example. Bending can be obtained from (44) by setting the stretches $\lambda_i = 1$, and all the angles to zero: $\varphi = \psi = \theta = \alpha = 0$, see Fig. 4. The curve (39) becomes

$$f_c(x_1) = R\sin\phi\,\mathbf{e}_1 + R(\cos\phi - 1)\mathbf{e}_3, \quad (48)$$

with $\phi = x_1/R$. The Frenet frame reads

$$\begin{aligned} \mathbf{t}(x_1) &= \cos\phi\,\mathbf{e}_1 - \sin\phi\,\mathbf{e}_3, \\ \mathbf{n}(x_1) &= -\sin\phi\,\mathbf{e}_1 - \cos\phi\,\mathbf{e}_3, \quad (49) \\ \mathbf{b}(x_1) &= \mathbf{e}_2, \end{aligned}$$

while curvature and torsion are given by $\kappa = 1/R$, $\tau = 0$. A surface f_s is obtained by extruding the curve (48) along the binormal direction $\mathbf{b} = \mathbf{e}_2$:

$$f_s(x_1, x_2) = -R(\mathbf{n}(x_1) + \mathbf{e}_3) + x_2\mathbf{e}_2. \quad (50)$$

Finally, the 3D volume f is obtained by extruding f_s along $\mathbf{n}_s = -\mathbf{n}$,

$$f(x_1, x_2, x_3) = -(R + x_3)\mathbf{n}(x_1) - R\mathbf{e}_3 + x_2\mathbf{e}_2, \quad (51)$$

with $\mathbf{n}_s = -\mathbf{n}$. The matrix representation of the gradient $\mathbf{F} = \nabla f$ of the embedding is

$$[\mathbf{F}] = \begin{bmatrix} \dfrac{(R + x_3)\cos\phi}{R} & 0 & \sin\phi \\ 0 & 1 & 0 \\ -\dfrac{(R + x_3)\sin\phi}{R} & 0 & \cos\phi \end{bmatrix}. \quad (52)$$

The corresponding metric $\mathbf{C} = \nabla f^\top \nabla f$ is

$$[\mathbf{C}] = \begin{bmatrix} \left(\dfrac{R + x_3}{R}\right)^2 & 0 & 0 \\ 0 & 1 & 0 \\ 0 & 0 & 1 \end{bmatrix}. \quad (53)$$

Finally, the stretch $\mathbf{U} = \sqrt{\mathbf{C}}$ is

$$[\mathbf{U}] = \begin{bmatrix} 1 + \dfrac{x_3}{R} & 0 & 0 \\ 0 & 1 & 0 \\ 0 & 0 & 1 \end{bmatrix}. \quad (54)$$

The metric (53) satisfies the compatibility condition (22) by construction; it follows that the stretch (54) describes a prototypical compatible distortion $\mathbf{U}_o = \mathbf{U}(R)$, parametrized by R; in particular, for $R \to \infty$, the distortion $\mathbf{U}_o \to \mathbf{I}$. Rewriting
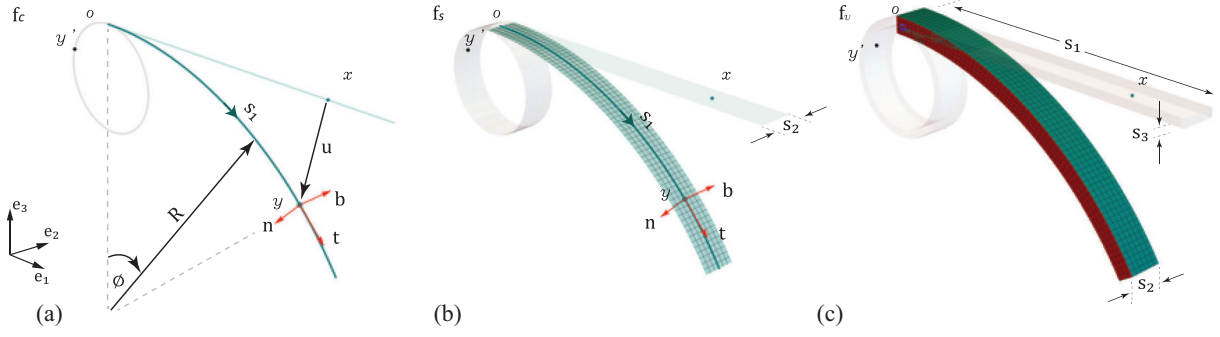
FIG. 4. From left to right: curve $f_c(s_1)$ around a cylinder; bent surface $f_s(s_1, s_2)$; bent solid $f(s_1, s_2, s_3)$.

(47) as $f(\mathscr{B}; R)$, we have

$$
\begin{aligned}
f(\mathscr{B}; \infty) &= \mathscr{B}, & \text{f is the identity map;} \\
f\left(\mathscr{B}; \frac{L}{2\pi}\right), & & \text{f yields a cylinder.}
\end{aligned}
\tag{55}
$$

To avoid self penetration we need $H/2 \leqslant R$. Figure 5 shows some bent configurations for the parallelepiped $\mathscr{B}$ with $H = L/\pi$ (top row) and $H = 2L/\pi$ (bottom row).

B. Special bending cases

Basing on the bending matrix (52), we now look for different distortion fields capable of yielding stress-free bending. These compatible fields are found by solving for $\mathbf{C}_o$ the equation $\mathbf{R}(\mathbf{C}_o) = 0$.

1. Bending induced by nematic distortions

Let us consider a distortion field $\mathbf{F}_o$ [26,27,50] representing a hybrid nematic orientation in the vertical plane; we have

$$
\begin{aligned}
\mathbf{F}_o &= \lambda_\parallel \mathbf{n} \otimes \mathbf{n} + \lambda_\perp (\mathbf{I} - \mathbf{n} \otimes \mathbf{n}) \\
&= \lambda_\perp \mathbf{I} + \lambda_a \mathbf{n} \otimes \mathbf{n},
\end{aligned}
\tag{56}
$$

where the director $\mathbf{n} = \cos \alpha(x_3)\mathbf{e}_1 + \sin \alpha(x_3)\mathbf{e}_3$ describes the nematic orientation, $\lambda_\parallel$ is the stretch parallel to the line $\mathbf{n} \otimes \mathbf{n}$, $\lambda_\perp$ is the stretch in the plane orthogonal to that line,
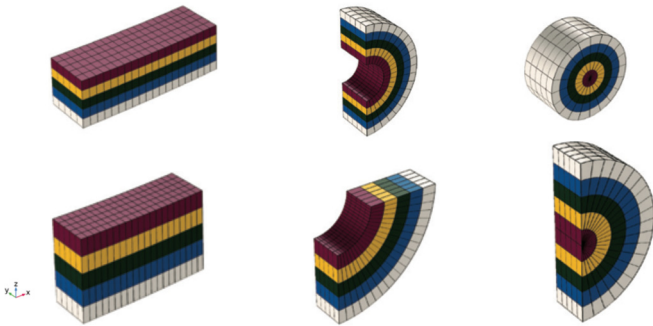

FIG. 5. Bending of a parallelepiped of length L and height H. (top row) $H = L/\pi$: the reference parallelepiped bends by π radians at $R = L/\pi$ and becomes a closed cylinder at $R = L/(2\pi)$. (bottom row) $H = 2L/\pi$: the reference parallelepiped bends by $\pi/2$ radians at $R = 2L/\pi$ and becomes a half cylinder at $R = L/\pi$, the minimum radius avoiding self-penetration. All six configurations are stress-free.

and $\lambda_a = \lambda_\parallel - \lambda_\perp$. The corresponding metric $\mathbf{C}_o$ is given by

$$
\begin{aligned}
\mathbf{C}_o &= \lambda_\parallel^2 \mathbf{n} \otimes \mathbf{n} + \lambda_\perp^2 (\mathbf{I} - \mathbf{n} \otimes \mathbf{n}) \\
&= \lambda_\perp^2 \mathbf{I} + \Lambda \mathbf{n} \otimes \mathbf{n},
\end{aligned}
\tag{57}
$$

with $\Lambda = \lambda_\parallel^2 - \lambda_\perp^2$. We use the compatibility condition (22) to characterize the nematic orientation $\alpha = \alpha(x_3)$ that makes $\mathbf{C}_o$ a compatible metric. The Riemann curvature $\mathbf{R}(\mathbf{C}_o)$ has five out of six null components

$$
\mathbf{R}_{1212} = \mathbf{R}_{1213} = \mathbf{R}_{1223} = \mathbf{R}_{1323} = \mathbf{R}_{2323} = 0.
\tag{58}
$$

It remains to solve for $\alpha = \alpha(x_3)$ the equation $\mathbf{R}_{1313} = 0$, with

$$
\mathbf{R}_{1313} = \Lambda \left(\cos(2\alpha)\alpha'^2 + \tfrac{1}{2} \sin(2\alpha)\alpha'' \right).
\tag{59}
$$

We assume anchoring conditions for the nematic orientation: a planar alignment at bottom, $\alpha(-H/2) = 0$, and a vertical one at top, $\alpha(H/2) = \pi/2$. It follows that the equation $\mathbf{R}_{1323} = 0$ is solved by

$$
\alpha(x_3) = \frac{1}{2} \arccos\left(-\frac{2x_3}{H} \right).
\tag{60}
$$

It is worth noting that the metric (57) with the orientation $\alpha(x_3)$ given by (60) is always compatible, for any value of $\lambda_\parallel, \lambda_\perp$, provided $\det(\mathbf{C}_o)$ remains positive.

Let us denote with $\tilde{\mathbf{F}}_o$ the distortion (56), and $\tilde{\mathbf{C}}_o$ the metric (57), where $\alpha(x_3)$ is given by (60); we have

$$
[\tilde{\mathbf{F}}_o] = \begin{bmatrix} \lambda_\perp + \lambda_a\left(\dfrac{1}{2} - \dfrac{x_3}{H}\right) & 0 & \dfrac{\lambda_a}{2}\sqrt{1 - \dfrac{4x_3^2}{H^2}} \\ & \lambda_\perp & 0 \\ \text{Sym} & & \lambda_\perp + \lambda_a\left(\dfrac{1}{2} - \dfrac{x_3}{H}\right) \end{bmatrix},
\tag{61}
$$

and

$$
[\tilde{\mathbf{C}}_o] = \begin{bmatrix} \lambda_\perp^2 + \Lambda\left(\dfrac{1}{2} - \dfrac{x_3}{H}\right) & 0 & \dfrac{\Lambda}{2}\sqrt{1 - \dfrac{4x_3^2}{H^2}} \\ & \lambda_\perp^2 & 0 \\ \text{Sym} & & \lambda_\perp^2 + \Lambda\left(\dfrac{1}{2} - \dfrac{x_3}{H}\right) \end{bmatrix}.
\tag{62}
$$

It is worth noting that the distortion field $\tilde{\mathbf{F}}_o$ has an explicit integral; that is, we can solve for $\tilde{f}$ the equation $\nabla \tilde{f} = \tilde{\mathbf{F}}_o$. We
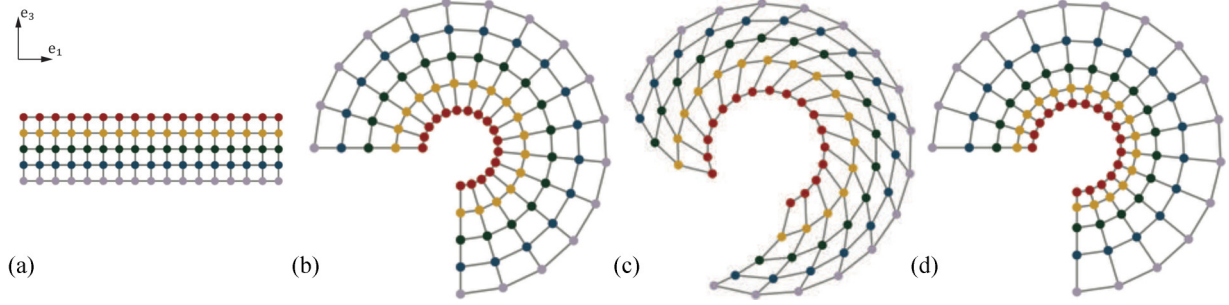
FIG. 6. We plot in the plane $\mathbf{e}_1 \wedge \mathbf{e}_3$ the cross sections of $\mathscr{B}$ and of its bent configurations, using a wire-frame plot to highlight the deformation. From left to right: reference cross section; classic bending from (54) with $R = 4/3 \times 1/(2\pi)$; nematic bending from (61) with $\Delta\beta = 3/4 \times 2\pi$; bending due the transverse isotropic distortion (67), with $c_1 = 1, c_2 = 3/4 \times 2\pi$. Plots are scaled differently.

find

$$\tilde{f}(x_1, x_2, x_3) = r(x_3)\mathbf{Q}(\beta(x_1, x_3))\mathbf{e}_3, \qquad (63)$$

with $\mathbf{Q}$ a rotation of angle $\beta = \beta_o(x_3) - x_1\beta_1$,

$$[\mathbf{Q}] = \begin{bmatrix} \cos\beta & 0 & -\sin\beta \\ 0 & 1 & 0 \\ \sin\beta & 0 & \cos\beta \end{bmatrix}. \qquad (64)$$

The functions $r(x_3)$, $\beta_o(x_3)$ and the parameter β_1, together with a sketch of their derivation are given in the Appendix B. Using the same notation as in (47), we have that $\tilde{f}(\mathscr{B}; \lambda_\parallel, \lambda_\perp)$ represents a bent, stress-free configuration of $\mathscr{B}$, which is a quite different kind of bending with respect to the one given by (54), see Fig. 6.

Given the function $\beta(x_1, x_3)$, we can evaluate the difference between the rotations at the two ends of the parallelepiped $\mathscr{B}$; we have

$$\Delta\beta = \beta(L, 0) - \beta(0, 0) = -\frac{L}{2H}\frac{\Lambda}{\lambda_\parallel \lambda_\perp}. \qquad (65)$$

When $\Delta\beta = \pm 2\pi$, the reference parallelepiped bends to a closed cylinder; as example, with $\lambda_\perp = 1$, we have

$$\Delta\beta = \pm 2\pi \Leftrightarrow \lambda_\parallel = \mp\frac{2\pi H}{L} + \sqrt{1 + \left(\frac{2\pi H}{L}\right)^2}. \qquad (66)$$

2. Bending induced by transverse-isotropic distortions

Let us consider the distortion field $\mathbf{F}_o = \mathbf{Q}_o\mathbf{U}_o$ defined by a rotation $\mathbf{Q}_o$ with axis $\mathbf{e}_2$, and a stretch $\mathbf{U}_o$ in the plane $\bar{\mathbf{I}} = \mathbf{I} - \mathbf{e}_2 \otimes \mathbf{e}_2$ orthogonal to that axis [13]:

$$\begin{aligned} \mathbf{Q}_o &= \mathbf{e}_2 \otimes \mathbf{e}_2 + \cos\alpha(x_1)\bar{\mathbf{I}} + \sin\alpha(x_1)\mathbf{e}_1 \wedge \mathbf{e}_3, \\ \mathbf{U}_o &= \mathbf{e}_2 \otimes \mathbf{e}_2 + \lambda(x_3)\bar{\mathbf{I}}. \end{aligned}$$

Its matrix-like representation is

$$[\mathbf{F}_o] = \begin{bmatrix} \lambda(x_3)\cos\alpha(x_1) & 0 & \lambda(x_3)\sin\alpha(x_1) \\ 0 & 1 & 0 \\ -\lambda(x_3)\sin\alpha(x_1) & 0 & \lambda(x_3)\cos\alpha(x_1) \end{bmatrix}, \qquad (67)$$

and the corresponding metric is

$$[\mathbf{C}_o] = \begin{bmatrix} \lambda(x_3)^2 & 0 & 0 \\ 0 & 1 & 0 \\ 0 & 0 & \lambda(x_3)^2 \end{bmatrix}. \qquad (68)$$

Also in this case, the Riemann curvature $\mathbf{R}(\mathbf{C}_o)$ has five out of six null components

$$\mathbf{R}_{1212} = \mathbf{R}_{1213} = \mathbf{R}_{1223} = \mathbf{R}_{1323} = \mathbf{R}_{2323} = 0. \qquad (69)$$

It remains to solve for $\lambda(x_3)$ the equation $\mathbf{R}_{1313} = 0$, with

$$\mathbf{R}_{1313} = \lambda'(x_3)^2 - \lambda(x_3)\lambda(x_3)''.$$

The equation $\mathbf{R}_{1313} = 0$ yields

$$\lambda(x_3) = c_1 \exp(c_2 x_3). \qquad (70)$$

It is easy to verify that a placement $\tilde{f}$ which realizes the distortion field (67) is given by

$$\tilde{f} = x_2\mathbf{e}_2 + \frac{1}{c_2}\lambda(x_3)[\sin(c_2 x_1)\mathbf{e}_1 + \cos(c_2 x_1)\mathbf{e}_3]. \qquad (71)$$

Rewriting (47) as $\tilde{f}(\mathscr{B}; c_1, c_2)$, we have

$$\begin{aligned} &\lim_{c_2 \to 0} \tilde{f}(\mathscr{B}; 1, c_2) = \mathscr{B}, \quad \tilde{f} \text{ is the identity map;} \\ &\tilde{f}(\mathscr{B}; 1, 2\pi), \qquad\qquad \tilde{f} \text{ yields a cylinder.} \end{aligned} \qquad (72)$$

C. Torsion

Torsion can be obtained from (44) by setting the stretches $\lambda_i = 1$, the angles $\varphi = \psi = \alpha = 0$, and the radius $R \to \infty$. The curve (39), the surface (42) and the volume (44) become

$$f_c(x_1) = x_1\mathbf{e}_1,$$

$$f_s(x_1, x_2) = x_1\mathbf{e}_1 + x_2(\cos\theta\mathbf{e}_2 + \sin\theta\mathbf{e}_3),$$

$$\begin{aligned} f(x_1, x_2, x_3) = x_1\mathbf{e}_1 &+ (x_2\cos\theta - x_3\sin\theta)\mathbf{e}_2 \\ &+ (x_2\sin\theta + x_3\cos\theta)\mathbf{e}_3. \end{aligned} \qquad (73)$$

Moreover, we assume $\theta = \theta_o + x_1/L\theta_1$; see Fig. 7. The matrix representation of the gradient ∇f is

$$[\mathbf{F}] = \begin{bmatrix} 1 & 0 & 0 \\ -a\theta_1 & \cos\theta & -\sin\theta \\ b\theta_1 & \sin\theta & \cos\theta \end{bmatrix}, \qquad (74)$$

with $a = (x_2\sin\theta + x_3\cos\theta)/L$ and $b = (x_2\cos\theta - x_3\sin\theta)/L$. The corresponding metric is

$$[\mathbf{C}] = \begin{bmatrix} 1 + \dfrac{\theta_1^2(x_2^2 + x_3^2)}{L^2} & \dfrac{-\theta_1 x_3}{L} & \dfrac{\theta_1 x_2}{L} \\ \dfrac{-\theta_1 x_3}{L} & 1 & 0 \\ \dfrac{\theta_1 x_2}{L} & 0 & 1 \end{bmatrix}. \qquad (75)$$
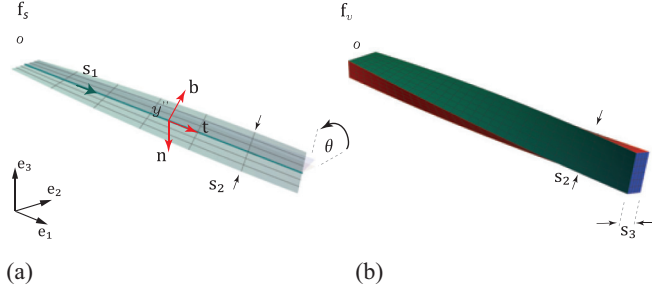
(a)   (b)

FIG. 7. The torsion given by the map $(73)_3$. (left) Surface f_s with the local Frenet frame shown at $y = f_s(x_1, x_2)$. (right) Solid f obtained by extruding f_s along $\mathbf{n}_s$.

The prototypical distortion $\mathbf{U}_o$ is defined as the square root of the metric tensor: $\mathbf{U}_o = \sqrt{\mathbf{C}}$; this square root has an explicit representation, and the six strict components of $\mathbf{U}_o$ are given in Appendix C.

This prototypical distortion $\mathbf{U}_o = \mathbf{U}_o(\theta_1)$ is parametrized by θ_1 and yields a torsion proportional to the length of the beam; following the notation (47), we have that $f(\mathcal{B}; \theta_1)$ represents a twisted parallelepiped whose base at $x_1 = L$ is rotated by θ_1 with respect to the base at $x_1 = 0$, see Fig. 8. Note that $\mathbf{U}(0) = \mathbf{I}$.

D. Helicoidal ribbons

We now use the general formula (44) to define some distortions $\mathbf{U}_o$ yielding different helicoidal ribbons; in particular, we focus on *flat ribbons*, corresponding to $\varphi = \psi$, having no shear ($\alpha = -\psi$) or sheared ($\alpha \neq \psi$), and to *saddle-ribbons* for which $\varphi \neq \psi$. Then, we investigate the compatibility of different $\bar{\mathbf{U}}_o$, obtained basing on the previously defined $\mathbf{U}_o$.

1. Flat ribbon without shear: $\varphi = \psi$, $\alpha = -\psi$

A particular helicoidal solid can be obtained from (44) by setting the stretches $\lambda_i = 1$, the angles $\varphi = \psi = \pi/4$, and $\alpha = -\psi = -\pi/4$; finally, the twist angle is null, $\theta = 0$. The curve (39) yields a helix around a cylinder of radius R; the surface (42) is developable and is given by

$$f_s(x_1, x_2) = \left(\frac{x_1 + x_2}{\sqrt{2}}\right)\mathbf{e}_1 + R(\cos\phi\,\mathbf{e}_2 + \sin\phi\,\mathbf{e}_3), \quad (76)$$

with $\phi = (x_1 - x_2)/(\sqrt{2}R)$. Then, the volume (44) is

$$f(x_1, x_2, x_3) = \left(\frac{x_1 + x_2}{\sqrt{2}}\right)\mathbf{e}_1 + (R + x_3)(\cos\phi\,\mathbf{e}_2 + \sin\phi\,\mathbf{e}_3). \quad (77)$$
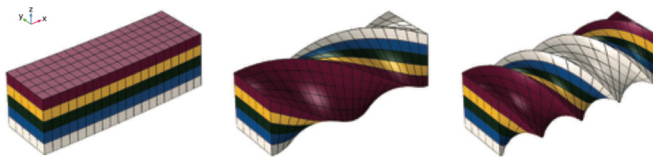

FIG. 8. (left to right) Reference parallelepiped; twisted configuration at $\theta_1 = \pi$; twisted configuration at $\theta_1 = 2\pi$. All three configurations are stress-free.

The gradient of (77) is given by

$$[\mathbf{F}] = \begin{bmatrix} \dfrac{1}{\sqrt{2}} & \dfrac{1}{\sqrt{2}} & 0 \\ -\dfrac{R+x_3}{\sqrt{2}R}\sin\phi & \dfrac{R+x_3}{\sqrt{2}R}\sin\phi & \cos\phi \\ \dfrac{R+x_3}{\sqrt{2}R}\cos\phi & -\dfrac{R+x_3}{\sqrt{2}R}\cos\phi & \sin\phi \end{bmatrix}, \quad (78)$$

and the corresponding metric is

$$[\mathbf{C}] = \begin{bmatrix} 1 + \dfrac{x_3}{R} + \dfrac{1}{2}\left(\dfrac{x_3}{R}\right)^2 & -\dfrac{x_3}{R} - \dfrac{1}{2}\left(\dfrac{x_3}{R}\right)^2 & 0 \\ -\dfrac{x_3}{R} - \dfrac{1}{2}\left(\dfrac{x_3}{R}\right)^2 & 1 + \dfrac{x_3}{R} + \dfrac{1}{2}\left(\dfrac{x_3}{R}\right)^2 & 0 \\ 0 & 0 & 1 \end{bmatrix}. \quad (79)$$

The prototypical distortion $\mathbf{U}_o = \sqrt{\mathbf{C}}$ is defined as the square root of the metric tensor (79); this square root has an explicit representation, and the six strict components of $\mathbf{U}_o$ are given by

$$U_{o11} = U_{o22} = \frac{1}{2}\left[1 + \sqrt{1 + 2\left(\frac{x_3}{R} + \frac{x_3^2}{2R^2}\right)}\right],$$

$$U_{o33} = 1,$$

$$U_{o12} = \frac{1}{2}\left[1 - \sqrt{1 + 2\left(\frac{x_3}{R} + \frac{x_3^2}{2R^2}\right)}\right],$$

$$U_{o13} = U_{o23} = 0. \quad (80)$$

2. Flat ribbon with shear: $\varphi = \psi$, $\alpha = 0$

A different helicoidal solid can be obtained from (44) by setting the stretches $\lambda_i = 1$, the angles $\varphi = \psi = \pi/4$, and $\alpha = \theta = 0$. The surface (42) is again developable, and given by

$$f_s(x_1, x_2) = \left(\frac{x_1}{\sqrt{2}} + x_2\right)\mathbf{e}_1 + R(\cos\phi\,\mathbf{e}_2 + \sin\phi\,\mathbf{e}_3), \quad (81)$$

with $\phi = x_1/(\sqrt{2}R)$. Then, the volume (44) is

$$f(x_1, x_2, x_3) = \left(\frac{x_1 + x_2}{\sqrt{2}}\right)\mathbf{e}_1 \qquad (82)$$
$$+ (R + x_3)(\cos\phi\,\mathbf{e}_2 + \sin\phi\,\mathbf{e}_3).$$

The gradient of (82) is given by

$$[\mathbf{F}] = \begin{bmatrix} \dfrac{1}{\sqrt{2}} & 1 & 0 \\ -\dfrac{R+x_3}{\sqrt{2}R}\sin\phi & 0 & \cos\phi \\ \dfrac{R+x_3}{\sqrt{2}R}\cos\phi & 0 & \sin\phi \end{bmatrix}, \quad (83)$$
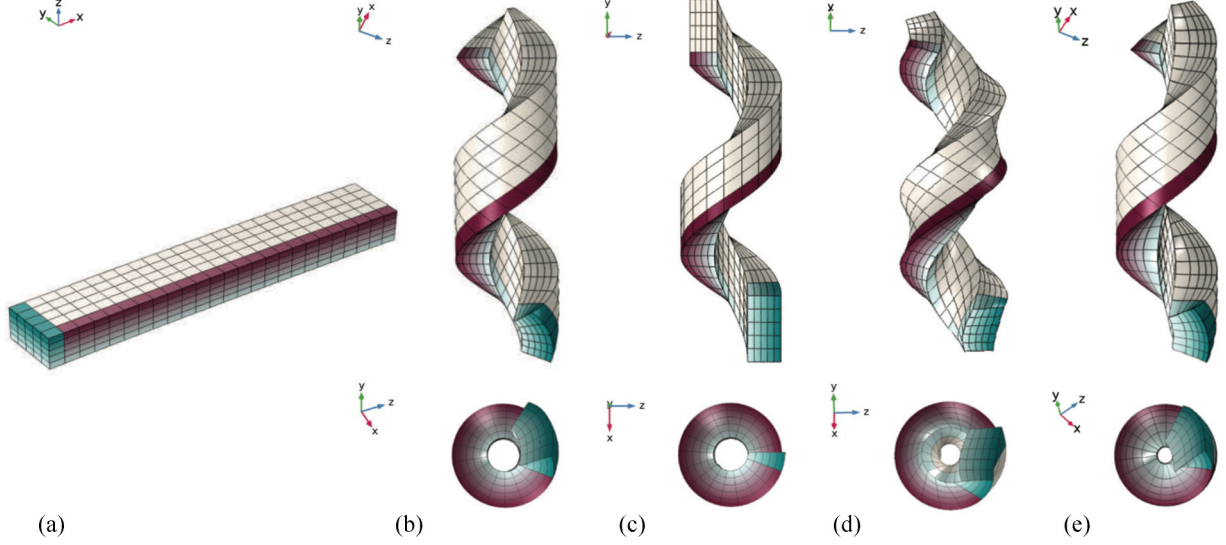
FIG. 9. Morphing of a thick parallelepiped due to compatible distortions fields; wire-frame and coloring are used to highlight the shape transformations. (a) Reference parallelepiped $\mathscr{B}$. (b) Flat and unsheared ribbon with $\varphi = \psi = \pi/4$ and $\alpha = -\psi = -\pi/4$. (c) Flat and sheared ribbon with $\varphi = \psi = \pi/4$ and $\alpha = 0$. (d) Saddle-ribbon with $\varphi = \pi/4$ and $\psi = \alpha = 0$. (e) Ribbon given by the compatible distortion (94) with the further request $\det(\tilde{\mathbf{U}}_o) = 1$. All the morphings are stress-free.

and the corresponding metric is

$$
[\mathbf{C}] = \begin{bmatrix} 1 + \dfrac{x_3}{R} + \dfrac{1}{2}\left(\dfrac{x_3}{R}\right)^2 & \dfrac{1}{\sqrt{2}} & 0 \\ \dfrac{1}{\sqrt{2}} & 1 & 0 \\ 0 & 0 & 1 \end{bmatrix}. \tag{84}
$$

The corresponding prototypical distortion $\mathbf{U}_o = \sqrt{\mathbf{C}}$ is defined as the square root of the metric tensor (84); this square root has an explicit representation, and the six strict components of $\mathbf{U}_o$ are given in Appendix D.

Both the distortions associated with (79) and to (84) are characterized by the parameter R; following notation (47), we have that $f(\mathscr{B}; R)$ represents a 3D helicoidal ribbon, see Figs. 9(b) and 9(c). Being $\varphi = \pi/4$, it follows that for $2\pi R = L\cos\varphi$ the ribbon completes a turn around the cylinder.

3. Saddle-ribbons: $\varphi \neq \psi$

Ribbons with a double curvature can be obtained from (44) by setting $\varphi \neq \psi$; here we analyze the case corresponding to $\lambda_i = 1$, the helix angle $\varphi = \pi/4$, and $\psi = \alpha = \theta = 0$. The surface (42) is not developable; for this case we give directly the six strict components of the corresponding metric tensor:

$$
\mathbf{C}_{11} = \frac{a^2 + (x_3\kappa)^2 + ax_3\kappa(x_3\kappa + 2\sqrt{a})}{a}, \tag{85}
$$

$$
\mathbf{C}_{22} = 1 + \left(\frac{x_3\kappa}{a}\right)^2, \tag{86}
$$

$$
\mathbf{C}_{33} = 1, \tag{87}
$$

$$
\mathbf{C}_{12} = -\frac{x_3\kappa(2a + x_3\kappa\sqrt{a})}{a^{3/2}}, \tag{88}
$$

$$
\mathbf{C}_{13} = \mathbf{C}_{23} = 0, \tag{89}
$$

with $a = 1 + (\kappa x_2)^2$. Also for this case, the corresponding prototypical distortion $\mathbf{U}_o = \sqrt{\mathbf{C}}$ has an explicit representation; we do not report the six strict components of $\mathbf{U}_o$, easily found with an algebraic manipulator such as Wolfram *Mathematica*. The effect of this distortion on the reference parallelepiped $\mathscr{B}$ is shown on Fig. 9(d).

4. Ribbon from $\mathbf{R}(\tilde{\mathbf{C}}_o) = 0$ (case A)

Basing on the distortion (80), we now look for different distortion fields capable of yielding a similar stress-free morphing. We start from the distortion field

$$
[\tilde{\mathbf{U}}_o] = \begin{bmatrix} \dfrac{1+b}{2} & \dfrac{1-b}{2} & 0 \\ \dfrac{1-b}{2} & \dfrac{1+b}{2} & 0 \\ 0 & 0 & 1 \end{bmatrix}, \tag{90}
$$

with $b = \sqrt{1 + 2g(x_3)}$, whose associated metric is

$$
[\tilde{\mathbf{C}}_o] = \begin{bmatrix} 1 + g(x_3) & -g(x_3) & 0 \\ -g(x_3) & 1 + g(x_3) & 0 \\ 0 & 0 & 1 \end{bmatrix}. \tag{91}
$$

We use the compatibility condition $\mathbf{R}(\tilde{\mathbf{C}}_o) = 0$ to characterize the class of functions $g(x_3)$ delivering a compatible metric. The Riemann curvature $\mathbf{R}(\tilde{\mathbf{C}}_o)$ has three out of six null components: $\mathbf{R}_{1212} = \mathbf{R}_{1213} = \mathbf{R}_{1223} = 0$; the remaining three components are given by

$$
\mathbf{R}_{1313} = \mathbf{R}_{1223} = \mathbf{R}_{2323} = \frac{g(x_3)'^2}{1 + 2g(x_3)} - g(x_3)''. \tag{92}
$$

Thus, by solving for $g(x_3)$ the equation $\mathbf{R}(\tilde{\mathbf{C}}_o) = 0$, we get

$$
g(x_3) = c_2 + x_3 c_1\left(1 + \frac{x_3 c_1}{2 + 4c_2}\right). \tag{93}
$$

The distortion (80) obtained directly from the embedding is recovered as a special case of (90) by setting $c_1 = 1/R$ and $c_2 = 0$ in (93).

5. Ribbon from $\mathbf{R}(\tilde{\mathbf{C}}_o) = 0$, with $\det(\tilde{\mathbf{U}}_o) = 1$ (case B)

Basing on the distortion (90), we consider

$$[\tilde{\mathbf{U}}_o] = \begin{bmatrix} \dfrac{1+b}{2} & \dfrac{1-b}{2} & 0 \\ \dfrac{1-b}{2} & \dfrac{1+b}{2} & 0 \\ 0 & 0 & 1+h(x_3) \end{bmatrix}, \quad (94)$$

whose metric is

$$[\tilde{\mathbf{C}}_o] = \begin{bmatrix} 1+g(x_3) & -g(x_3) & 0 \\ -g(x_3) & 1+g(x_3) & 0 \\ 0 & 0 & [1+h(x_3)]^2 \end{bmatrix}. \quad (95)$$

The Riemann curvature $\mathbf{R}(\tilde{\mathbf{C}}_o)$ has three out of six null components: $\mathbf{R}_{1212} = \mathbf{R}_{1213} = \mathbf{R}_{1223} = 0$. The remaining three components are equal, $\mathbf{R}_{1313} = \mathbf{R}_{1323} = \mathbf{R}_{2323}$, and are given by

$$\mathbf{R}_{1313} = \frac{1}{2}\left(\frac{g(x_3)'^2}{1+2g(x_3)} + \frac{g(x_3)' h(x_3)'}{1+h(x_3)} - g(x_3)'' \right). \quad (96)$$

Thus, by solving for $h(x_3)$ the equation $\mathbf{R}(\tilde{\mathbf{C}}_o) = 0$, we find that the compatibility request is fulfilled whenever

$$h(x_3) = \frac{c_3 g(x_3)'}{\sqrt{1+2g(x_3)}} - 1. \quad (97)$$

By adding the request of a volume-preserving morphing, we can characterize the function $g(x_3)$; we have

$$\det(\tilde{\mathbf{U}}_o) = 1 \Rightarrow c_3 g(x_3)' = 1 \Rightarrow g(x_3) \text{ linear}. \quad (98)$$

Here, we assume $g(x_3) = x_3/R$; then (98) implies $c_3 = R$, and $\tilde{U}_{o33} = 1/\sqrt{1+2x_3/R}$. The corresponding morphing is shown in Fig. 9(e).

6. Thick tube formation

Some of the distortions of Sec. V D can morph a parallelepiped $\mathscr{B}$ into a closed, thick tube, which is stress free. For the flat ribbons ($\varphi = \psi$), tube formation is described by two equations:

$$\text{Side match:} \quad w_a = 2\pi R \sin\varphi, \quad (99)$$

$$\text{\# of turns:} \quad \beta 2\pi R = L\cos\varphi, \quad (100)$$

where w_a is the actual width of the ribbon, see Fig. 10. As example, let $L = 2\pi$, $W = \pi$ and set $\varphi = \pi/4$; for $\alpha = -\varphi$, we have $w_a = W$ and we solve (99) for the curvature radius R and the number of turns β: we get

$$\text{Side match:} \quad R = \frac{w_a}{2\pi \sin\varphi} = \frac{W}{2\pi}\sqrt{2} = \frac{1}{\sqrt{2}}, \quad (101)$$

$$\text{\# of turns:} \quad \beta = \frac{L\cos\varphi}{2\pi R} = 1. \quad (102)$$

For $\alpha = 0$, we have $w_a = W\cos\varphi$, and we get

$$\text{Side match:} \quad R = \frac{W\cos\varphi}{2\pi \sin\varphi} = \frac{1}{2}, \quad (103)$$

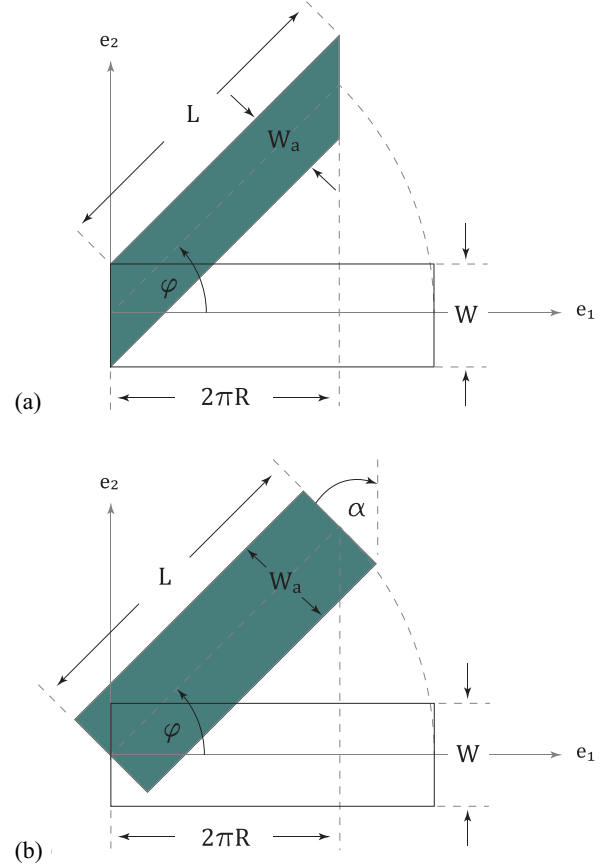
FIG. 10. We plot the image of the rectangle $L \times W$ given by the surface embedding (42), for $R \to \infty$ and $\varphi = \psi = \pi/4$. (top) $\alpha = 0$: the effective width of the sheared rectangle is $W_a = W\cos\varphi$. (bottom) $\alpha = -\pi/4$: the effective width of the un-sheared rectangle is $W_a = W$.

$$\text{\# of turns:} \quad \beta = \frac{L\cos\varphi}{2\pi R} = \sqrt{2}. \quad (104)$$

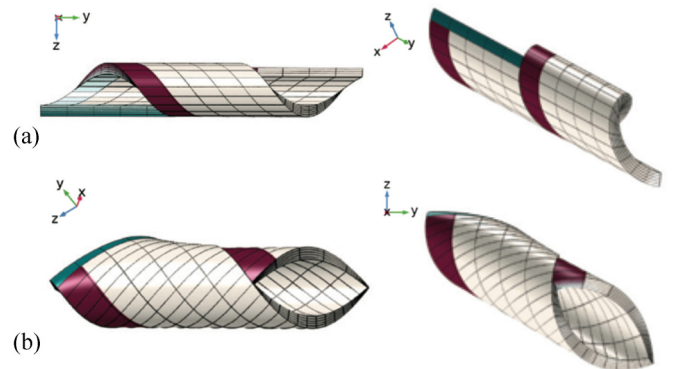Figure 11 shows the two configurations described by the previous equations.

FIG. 11. Stress-free tubes obtained by morphing a flat ribbon with $\varphi = \psi = \pi/4$. (a) Sheared ribbon: for $\alpha = 0$ and $R = 1/2$, the ribbon makes $\sqrt{2}$ turns around the cylinder. (b) Un-sheared ribbon: for $\alpha = -\pi/4$ and $R = 1/\sqrt{2}$, the ribbon makes 1 turn.

VI. CONCLUSIONS

There are plenty of papers dealing with the morphing of 2D elastic bodies; here we present a procedure aimed at designing the morphing of 3D bodies, with very large shape-changes in response to varying distortion fields, while keeping their stress state almost null. We focused on a class of distortions that have an explicit representation; nevertheless the method proposed here can be generalized to more complex geometries, and the families of morphings that can be generated is limitless.

This study has been motivated by the following, practical goal: realize an actuator or in general a shape transformation towards a target shape, which produces as less stress as possible, and ideally, no stress at all. In general, in a given material, the local deformation cannot be exactly equal to the assigned distortion, and thus distortions yield stress. Here we show that it is possible to design a compatible distortion field that induces in the body an immersion very similar to the desired one.

Actual examples of materials bodies capable of such controlled morphings are the nematic elastomers, whose transversally isotropic distortions are sensitive to temperature. For such materials, the global shape achieved at a given temperature is consequence of the local orientation of the nematic director.

In particular, living organisms provides many examples of both 2D and 3D morphings; the 3D study presented here might give new clues about the growing processes in biology and help to understand how stress can be controlled during growth.

Our design algorithm for stress-free morphing is based on two steps: at first we construct a family of 3D embeddings that can generate a great collection of different parametric configurations; from these embeddings it is possible to obtain prototypical distortion fields which are compatible by construction. The second step consists in modifying these prototypical distortions and solve the Riemann curvature equation to make them compatible again; as a result, we obtain many different distortion field capable of deforming a solid at zero stress. This procedure has been extensively illustrated by means of a variety of examples, and tested with finite element analyses.

ACKNOWLEDGMENTS

APPENDIX A: REPRESENTATION OF VECTORS AND TENSORS

Let $\{o; \mathbf{e}_1, \mathbf{e}_2, \mathbf{e}_3\}$ be an Euclidean frame, with orthonormal basis: $\mathbf{e}_i \cdot \mathbf{e}_j = \delta_{ij}$. Then, a basis of Lin is given by $\mathbf{e}_j \otimes \mathbf{e}_i$, with $i, j = 1, 2, 3$. The action of a simple tensor $\mathbf{u} \otimes \mathbf{v}$ on a vector $\mathbf{w}$ is given by

$$(\mathbf{u} \otimes \mathbf{v})\mathbf{w} = (\mathbf{v} \cdot \mathbf{w})\mathbf{u}. \tag{A1}$$

Vectors and tensors will be represented as linear combinations of basis elements or as matrices, according to convenience; as example for vectors:

$$\mathbf{v} = v_i \mathbf{e}_i \Leftrightarrow [\mathbf{v}] = \begin{bmatrix} v_1 \\ v_2 \\ v_3 \end{bmatrix}, \tag{A2}$$

and for tensors:

$$\mathbf{A} = A_{ij}\mathbf{e}_i \otimes \mathbf{e}_j \Leftrightarrow [\mathbf{A}] = \begin{bmatrix} A_{11} & A_{12} & A_{13} \\ A_{21} & A_{22} & A_{23} \\ A_{31} & A_{32} & A_{33} \end{bmatrix}. \tag{A3}$$

APPENDIX B: INTEGRATION OF THE NEMATIC DISTORTIONS

Given the ansatz (63) for the embedding f_o, we start by computing the associated metric $\mathbf{C} = \nabla f_o^T \nabla f_o$; its nontrivial strict components are

$$\begin{aligned} C_{11} &= \beta_1^2 r(x_3)^2, \\ C_{33} &= [r(x_3)\beta_o'(x_3)]^2 + r'(x_3)^2, \\ C_{13} &= r(x_3)^2 \beta_1 \beta_o'(x_3). \end{aligned} \tag{B1}$$

The request $\mathbf{C} = \mathbf{C}_o$ yields

$$r(x_3) = \pm \sqrt{\frac{\mathbf{C}_{o11}}{\beta_1^2}},$$

$$\beta_o'(x_3) = \pm \sqrt{\frac{\mathbf{C}_{o22} - r'(x_3)^2}{r(x_3)^2}} = \frac{\mathbf{C}_{o13}}{\beta_1 r(x_3)^2}. \tag{B2}$$

Substituting (B2)$_1$ into (B2)$_2$, we find β_1:

$$\beta_1 = \frac{1}{2H}\left(\frac{\lambda_\parallel^2}{\lambda_\perp^2} - \frac{\lambda_\perp^2}{\lambda_\parallel^2}\right). \tag{B3}$$

Finally, the integration of (B2)$_2$ yields, up to a constant,

$$\begin{aligned} \beta_o(x_3) &= -\frac{\lambda_\parallel^2 + \lambda_\perp^2}{2\lambda_\parallel^2 \lambda_\perp^2}\left[\mathbf{C}_{o13} + \frac{\lambda_\parallel^2 + \lambda_\perp^2}{2}\arcsin\left(\frac{2x_3}{H}\right)\right] \\ &\quad + \frac{\lambda_\parallel^2 + \lambda_\perp^2}{2\lambda_\parallel \lambda_\perp}\arctan(a). \end{aligned} \tag{B4}$$

and

$$a = \left(\frac{\Lambda}{2} + \frac{(\lambda_\parallel^2 + \lambda_\perp^2)x_3}{H}\right)\bigg/\left(\lambda_\parallel \lambda_\perp \sqrt{1 - \frac{4x_3^2}{H^2}}\right). \tag{B5}$$

APPENDIX C: SQUARE ROOT OF THE TORSION METRIC

The target metric (75) corresponds to a torsion; its square root $\mathbf{U}_o = \sqrt{\mathbf{C}_o}$ has the following explicit representation. Diagonal terms:

$$\begin{aligned} U_{o11} &= \frac{1}{2\sqrt{2}L}\left[\frac{\theta_1\sqrt{2}A_d}{\sqrt{D}} + A_s\right], \\ U_{o22} &= \frac{x_2^2}{r} + \frac{2L^2 + A^+A^-}{\sqrt{2}LrA_s}x_3^2, \\ U_{o33} &= \frac{x_3^2}{r} + \frac{2L^2 + A^+A^-}{\sqrt{2}LrA_s}x_2^2; \end{aligned} \tag{C1}$$

off-diagonal terms:

$$U_{o12} = \frac{A_d}{\sqrt{2rD}} x_3,$$

$$U_{o13} = -\frac{A_d}{\sqrt{2rD}} x_3,$$

$$U_{o23} = \frac{y x_3}{L} \left[\frac{L}{r} - \frac{2L^2 + A^+ A^-}{\sqrt{2} r A_s} \right]; \qquad \text{(C2)}$$

where $r = x_2^2 + x_3^2$, and

$$A_s = A^+ + A^-, \quad A_d = A^+ - A^-,$$

$$A^+ = \sqrt{2L^2 + B + C}, \quad A^- = \sqrt{2L^2 + B - C},$$

$$B = r\theta_1^2, \quad C = \sqrt{BD},$$

$$D = 4L^2 + B.$$

APPENDIX D: SQUARE ROOT OF THE METRIC OF THE FLAT RIBBON WITH SHEAR

The target metric (84) corresponds to a 3D helicoidal ribbon; its square root $\mathbf{U}_o = \sqrt{\mathbf{C}_o}$ has the following explicit representation:

$$U_{o11} = \frac{\sqrt{a_1 + a_2}(a_1 + a_3) + \sqrt{a_2 - a_1}(a_1 - a_3)}{4 a_1 R},$$

$$U_{o22} = \frac{\sqrt{a_2 - a_1}(a_1 + a_3) + \sqrt{a_2 + a_1}(a_1 - a_3)}{4 a_1 R},$$

$$U_{o12} = \frac{\sqrt{2} R}{\sqrt{a_1 + a_2} + \sqrt{a_2 - a_1}},$$

$$U_{o33} = 1, \quad U_{o13} = U_{o23} = 0, \qquad \text{(D1)}$$

with

$$a_1 = \sqrt{8R^4 + 4R^2 x_3^2 + 4R x_3^3 + x_3^4},$$

$$a_2 = 4R^2 + 2R x_3 + x_3^2,$$

$$a_3 = 2R x_3 + x_3^2. \qquad \text{(D2)}$$

[1] G. G. Stoney, The tension of metallic films deposited by electrolysis, Proc. R. Soc. A **82**, 172 (1909).

[2] S. Timoshenko, Analysis of bi-metal thermostats, J. Opt. Soc. Am. **11**, 233 (1925).

[3] B. Bilby, R. Bullough, E. Smith, and J. Whittaker, Continuous distributions of dislocations: a new application of the methods of non-Riemannian geometry, Proc. R. Soc. London, Ser. A **231**, 263 (1955).

[4] E. Kröner, Allgemeinen kontinuumstheorie der versetzungen und eigenspannungen, Arch. Rat. Mech. Anal. **4**, 273 (1959).

[5] E. Lee and D. Liu, Finite-strain elastic-plastic theory with application to plane-wave analysis, J. Appl. Phys. **38**, 19 (1967).

[6] E. Lee, Elastic-plastic deformation at finite strains, J. Appl. Mech. **36**, 1 (1969).

[7] S. Sadik and A. Yavari, On the origins of the idea of the multiplicative decomposition of the deformation gradient, Math. Mech. Solids **22**, 771 (2017).

[8] C. Eckart, The thermodynamics of irreversible processes. IV. The theory of elasticity and anelasticity, Phys. Rev. **73**, 373 (1948).

[9] A. DiCarlo and S. Quiligotti, Growth and balance, Mech. Res. Commun. **29**, 449 (2002).

[10] M. Minozzi, P. Nardinocchi, L. Teresi, and V. Varano, Growth-induced compatible strains, Math. Mech. Solids **22**, 62 (2017).

[11] Y. Klein, E. Efrati, and E. Sharon, Shaping of elastic sheets by prescription of non-euclidean metrics, Science, **315** 1116 (2007).

[12] E. Sharon, and E. Efrati, The mechanics of non-Euclidean plates, Soft Matter **6**, 5693 (2010).

[13] P. Nardinocchi, L. Teresi, and V. Varano, The elastic metric: A review of elasticity with large distortions, Int. J. Non-Linear Mech. **56**, 34 (2013).

[14] E. Rodriguez, A. Hoger, A. McCulloch, Stress dependent finite growth in soft elastic tissues, J. Biomech. **27**, 455 (1994).

[15] P. Nardinocchi, L. Teresi, On the active response of soft living tissues, J. Elasticity **88**, 27 (2007).

[16] A. Goriely, *The Mathematics and Mechanics of Biological Growth* (Springer, 2017), Vol. 45.

[17] D. Ambrosi, M. Ben Amar, C. J. Cyron, A. DeSimone, A. Goriely, J. D. Humphrey, and E. Kuhl, Growth and remodelling of living tissues: Perspectives, challenges and opportunities, J. R. Soc., Interface **16**, 20190233 (2019).

[18] S. Sadik, A. Angoshtari, A. Goriely, and A. Yavari, A geometric theory of nonlinear morphoelastic shells, J. Nonlinear Sci. **26**, 929 (2016).

[19] D. Grossman, E. Sharon, and E. Katzav, Shape and fluctuations of positively curved ribbons, Phys. Rev. E **98** 022502 (2018).

[20] E. Siéfert, I. Levin, and E. Sharon, Euclidean Frustrated Ribbons, Phys. Rev. X **11**, 011062 (2021).

[21] R. M. Erb, J. S. Sander, R. Grisch, and A. R. Studart, Self-saping composites with programmable bioinspired microstructures, Nat. Commun. **4**, 1712 (2013).

[22] C. Modes and M. Warner, Shape-programmable materials, Phys. Today **69**(1), 32 (2016).

[23] H. Aharoni, Y. Xia, X. Zhang, R. D. Kamien, S. Yang, Universal inverse design of surfaces with thin nematic elastomer sheets, Proc. Natl. Acad. Sci. USA **115**, 7206 (2018).

[24] T. van Manen, S. Janbaz, and A. A. Zadpoor, Programming 2D/3D shape-shifting with hobbyist 3D printers, Mater. Horiz. **4**, 1064 (2017).

[25] A. DeSimone and L. Teresi, Elastic energies for nematic elastomers, Eur. Phys. J. E: Soft Matter Biol. Phys. **29**, 191 (2009).

[26] Y. Sawa, K. Urayama, T. Takigawa, A. DeSimone, and L. Teresi, Thermally driven giant bending of liquid crystal elastomer films with hybrid alignment, Macromolecules (Washington, DC, US) **43**, 4362 (2010).

[27] L. Teresi, V. Varano, Modeling helicoid to spiral-ribbon transitions of twist-nematic elastomers, Soft Matter **9**, 3081 (2013).

[28] Y. Sawa, F. Ye, K. Urayamaa, T. Takigawa, V. Gimenez-Pinto, R. L. B. Selinger, and J. V. Selinger, Shape selection of twist-nematic-elastomer ribbons, Proc. Natl. Acad. Sci. USA **108**, 6364 (2011).

[29] C. Mostajeran, M. Warner, T. H. Ware, T. J. and White, Encoding Gaussian curvature in glassy and elastomeric liquid crystal solids, Proc. R. Soc. London, Ser. A **472**, 20160112 (2016).

[30] M. Warner, Topographic mechanics and applications of liquid crystalline solids, Annu. Rev. Condens. Matter Phys. **11**, 125 (2020).

[31] A. S. Kuenstler, Y. Chen, P. Bui, H. Kim, A. DeSimone, L. Jin, and R. C. Hayward, Blueprinting photothermal shape-morphing of liquid crystal elastomers, Adv. Mater. **32**, 2000609 (2020).

[32] P. Nardinocchi, L. Teresi, and V. Varano, Strain induced shape formation in fibred cylindrical tubes, J. Mech. Phys. Solids **60**, 1420 (2012).

[33] C. Dawson, J. F. Vincent, and A. M. Rocca, How pine cones open, Nature (London) **390**, 668 (1997).

[34] S. Armon, E. Efrati, R. Kupferman, and E. Sharon, Geometry and mechanics in the opening of chiral seed pods, Science **333**, 1726 (2011).

[35] R. Chelakkot and L. Mahadevan, On the growth and form of shoots, J. R. Soc., Interface **14**, 20170001 (2017).

[36] D. Agostinelli, A. Lucantonio, G. Noselli, and A. DeSimone, Nutations in growing plant shoots: The role of elastic deformations due to gravity loading, J. Mech. Phys. Solids **136**, 103702 (2020).

[37] J. M. McCracken, B. R. Donovan, and T. J. White, Materials as machines, Adv. Mater. **32**, 1906564 (2020).

[38] S. Poppinga, C. Zollfrank, O. Prucker, J. Rühe, A. Menges, T. Cheng, and T. Speck, Toward a new generation of smart biomimetic actuators for architecture, Adv. Mater. **30**, 1703653 (2018).

[39] L. K. Rivera-Tarazona, V. D. Bhat, H. Kim, Z. T. Campbell, and T. H. Ware, Shape-morphing living composites, Sci. Adv. **6**, eaax8582 (2020).

[40] P. G. Ciarlet, An introduction to differential geometry with applications to elasticity, J. Elasticity **78-79**, 1 (2005).

[41] C. Davini, Some remarks on the continuum theory of defects in solids, Int. J. Solids Struct. **38**, 1169 (2001).

[42] M. do Carmo, *Riemannian Geometry* (Birkhäuser, 1992).

[43] A. Yavari, Compatibility equations of nonlinear elasticity for non-simply-connected bodies, Arch. Ration. Mech. Anal. **209**, 237 (2013).

[44] A. E. H. Love *A Treatise on the Mathematical Theory of Elasticity* (Dover Publications, 1944).

[45] G. Tomassetti and V. Varano, Capturing the helical to spiral transitions in thin ribbons of nematic elastomers, Meccanica **52**, 3431 (2017).

[46] R. Paroni and G. Tomassetti, Macroscopic and microscopic behavior of narrow elastic ribbons, J. Elasticity **135**, 409 (2019).

[47] H. Singh and E. G. Virga, A ribbon model for nematic polymer networks, J. Elast. (2022).

[48] M. A. Dias and B. Audoly, ''Wunderlich, Meet Kirchhoff'': A general and unified description of elastic ribbons and thin rods, J. Elasticity **119**, 49 (2015).

[49] S. Gabriele, N. Rizzi, and V. Varano, A 1D higher gradient model derived from Koiter's shell theory, Math. Mech. Solids **21**, 737 (2016).

[50] M. Warner, C. Mostajeran, Nematic director fields and topographies of solid shells of revolution, Proc. R. Soc. London, Ser. A **474**, 20170566 (2018).